Phys Chem Minerals (2006) 33: 457–464
DOI 10.1007/s00269-006-0090-1

ORIGINAL PAPER

L. Cemič · E. Dachs

Heat capacity of ferrosilite, $Fe_2Si_2O_6$

Received: 16 November 2005 / Accepted: 11 May 2006 /

Abstract The heat capacity of synthetic ferrosilite, $Fe_2Si_2O_6$, was measured between 2 and 820 K. The physical properties measurement system (PPMS, Quantum Design®) was used in the low-temperature region between 2 and 303 K. In the temperature region between 340 and 820 K measurements were performed using differential scanning calorimetry (DSC). The C_p data show two transitions, a sharp λ-type at 38.7 K and a small shoulder near 9 K. The λ-type transition can be related to collinear antiferromagnetic ordering of the Fe^{2+} spin moments and the shoulder at 10 K to a change from a collinear to a canted-spin structure or to a Schottky anomaly related to an electronic transition. The C_p data in the temperature region between 145 and 830 K are described by the polynomial

$$C_p\left[\mathrm{J\,mol^{-1}\,K^{-1}}\right] = 371.75 - 3219.2T^{-1/2} - 15.199 \times 10^5 T^{-2} + 2.070 \times 10^7 T^{-3}$$

The heat content $[H_{298} - H_0]$ and the standard molar entropy $[S_{298} - S_0]$ are 28.6 ± 0.1 kJ mol^{-1} and 186.5 ± 0.5 J mol^{-1} K^{-1}, respectively. The vibrational part of the heat capacitiy was calculated using an elastic Debye temperature of 541 K. The results of the calculations are in good agreement with the maximum theoretical magnetic entropy of 26.8 J mol^{-1} K^{-1} as calculated from the relationship 2*Rln5.

Keywords Ferrosilite · Heat capacity · Magnetic transition

Introduction

Orthopyroxenes are rock-forming minerals found in the Earth's crust and upper mantle. Knowledge of their P-T-X behavior is, therefore, essential to geoscientists. Most orthopyroxenes are solid solutions between the two end-members $Mg_2Si_2O_6$ and $Fe_2Si_2O_6$. Hence, reliable thermodynamic data for both $Mg_2Si_2O_6$ and $Fe_2Si_2O_6$ are required in order to phase equilibria involving orthopyroxenes. Ferrosilite is not stable at low pressure, which probably explains the scarcity of thermodynamic data for it. The existing data for it were obtained from analyzing experimental phase equilibrium results (e.g. Holland and Powell 1998; Berman 1988). Bohlen et al. (1983) measured the heat capacity of ferrosilite in the temperature range between 8 and 350 K using intermittent heating adiabatic calorimetry. From their C_p data, they calculated the conventional standard entropy, $S_{298.15}$ and obtained a value of 189.12 J mol^{-1} K^{-1} (22.6 cal mol^{-1} K^{-1} based on half of the formula unit of ferrosilite, i.e., $FeSiO_3$). Their data showed a λ transition at 39 K that was attributed to antiferromagnetic spin ordering. No detailed data of C_p as a function of temperature are given in the publication. To the best of our knowledge, no experimentally determined heat capacity data for ferrosilite at temperatures above 350 K have been published.

Experimental

Samples

Ferrosilite was synthesized from synthetic fayalite, Fe_2SiO_4, and amorphous SiO_2 (Aerosil, Degussa, heated at 1,000°C for 24 h) at 800°C and 1.5 GPa in a piston-cylinder apparatus using the double-capsule technique. Fayalite was synthesised from Fe powder (Merck), Fe_2O_3 powder (Merck) and amorphous SiO_2. A mixture of the reactants, in proportions according to

L. Cemič (✉)
Institut für Geowissenschaften, Abteilung Mineralogie,
Christian-Albrechts-Universität zu Kiel,
Ludewig-Mayn-Str. 10, 24098 Kiel, Germany
E-mail: lc@min.uni-kiel.de
Tel.: +49-431-8801451
Fax: +49-431-8804457

E. Dachs
Fachbereich Materialwissenschaten, Universität Salzburg,
Hellbrunnerstr 34, 5020 Salzburg, Austria

the chemical reaction: $2Fe + 2Fe_2O_3 + 3SiO_2 = 3Fe_2SiO_4$, was pressed to a pellet and sealed into an evacuated SiO_2 glass ampoule. The ampoule was then heated to 800°C and for 48 h.

A mechanical mixture of SiO_2 and fayalite was welded into a silver capsule together with a small amount (< 0.5 µl) of destilled water. This capsule was then inserted into a larger gold capsule containing an iron/wustite (IW) mixture and water. The IW buffer was used to keep the oxygen fugacity low in order to prevent the formation of ferric iron. Strictly stoichiometric starting mixtures yielded, in addition to ferrosilite, also small amounts of fayalite. Apparently, SiO_2 dissolved preferentially in the fluid phase during synthesis, which then allowed the formation of a small amount of fayalite. The amount of SiO_2 was, therefore, increased successively until single-phase ferrosilite was obtained as a final product (i.e., a SiO_2 excess of ca. 10 mol% was needed to prevent the formation of fayalite).

The synthetic product was examined by optical microscopy, X-ray powder diffraction (XRD), electron microprobe analysis and Moessbauer spectroscopy. It showed a complete reaction and no Fe^{3+} was detected. An XRD pattern was collected with an automated diffractometer (Siemens D 5000) between 8 and 100° 2Θ using Cu-K_α radiation. The step size was 0.016° and the measuring time 11 s per step. The lattice parameters were refined with the Rietveld program Fullprof (Rodriguez-Carvajal 1990). The least-squares fit yielded the following values: $a = 18.425 \pm 0.004$ Å, $b = 9.073 \pm 0.002$ Å and $c = 5.237 \pm 0.002$ Å, compared to $a = 18.427 \pm 0.004$ Å, $b = 9.076 \pm 0.002$ Å and $c = 5.237 \pm 0.001$ Å as given by Sasaki et al. (1982). The refinement gave final values of 5.38 and 1.724 for R_{wp} and χ^2, respectively.

The composition of ferrosilite was determined with an electron microprobe (Jeol JXA 8900 R) operating in wavelength-dispersive mode with 15 kV excitation voltage, 15 nA beam current and 1–2 µm beam diameter. Synthetic fayalite and wollastonite were used as standards for iron and silicon, respectively. Analyses were made on ten different grains. The averaged values are 45.83 ± 0.14 for SiO_2 and 54.83 ± 0.39 wt% for FeO.

For the Mössbauer measurements, a $^{57}Co/Rh$ source (ca. 1.85 GBq) was used to generate 14.4 keV gamma rays. The spectrum was collected in constant acceleration mode at the temperature of liquid nitrogen (ca. 77 K). The absorber was prepared by mixing 19.80 mg of ferrosilite with 203.36 mg of cellulose (avicel). Two doublets resulting from Fe^{2+} at the M1 and M2 sites were observed. Four different lines were fit to the experimental spectrum using the fit program MOESALZ (Lottermoser et al. unpublished). The following parameters were determined: the quadrupole splitting values for the M1 and M2 sites were 3.128 and 1.995 mm s^{-1}, respectively. The isomer shift for M1 is 1.411 mm s^{-1} and that for M2 is 1.365 mm s^{-1} . The goodness of fit χ^2 was 1.49. These values can be compared with 3.181 mm s^{-1} (M1) and 2.021 mm s^{-1} (M2) for the quadrupole splitting and with 1.322 mm s^{-1} (M1) and 1.279 mm s^{-1} (M2) for the isomer sift, respectively, as given in Domeneghetti and Steffen (1992). No evidence for Fe^{3+} in the spectra was found.

The ferrosilite was sieved to produce a grain size fraction ranging between 0.125 and 0.355 mm for the calorimetric experiments.

Calorimetry

Low-temperature heat capacities were measured with the heat capacity option of the physical properties measurement system (PPMS) at Salzburg University. Based on heat-pulse calorimetry (e.g. Hwang et al. 1997), the PPMS is the first commercially available apparatus that can measure the low-temperature heat capacity of milligram-sized samples. For the heat capacity measurements, a 19.73 mg powdered sample of ferrosilite was sealed into small flat Al pans with lids and placed on the 4 × 4 mm wide sample platform of the PPMS calorimeter. One measurement was performed on heating from 2 to 303 K with 52 data points, each measured three times, and using a logarithmic spacing (Table 1, PPMS first series). Another series of measurements was made from 30 to 50 K at 40 evenly distributed set points of temperature around the sharp λ-type C_p anomaly (Fig. 2, Table 1, PPMS 2nd series). A detailed description of heat capacity measurements using the PPMS and an error analysis is given in Dachs and Bertoldi (2005).

In the temperature region between 340 and 820 K the measurements were made with a Perkin Elmer DSC 7. The experimental technique was similar to that described in Bosenick et al. (1996). The calorimeter block was kept at a constant temperature of 293 ± 3 K using dried nitrogen gas. The melting point of In at 429.75 K and the phase transition of Li_2SO_4 at 851.43 K (Cammenga et al. 1992) were used to calibrate the temperature. The temperature accuracy is assumed to be ± 1 K as determined by Bosenick et al. (1996). Single-crystal synthetic corundum was used as the C_p standard. Its heat capacity was taken from the National Bureau of Standards, USA. The standard (61.91 mg) and the sample (50–60 mg) were contained in Au pans.

The measurements were performed using the step-scanning method as described by Bosenick et al. (1996) with a heating rate of 20 K per minute over 100 K temperature intervals.

Results

The experimental results are listed in Table 1 and are shown graphically in Figs. 1 and 2. The heat capacity as a function of temperature shows two transitions, a sharp λ transition at 38.4 K and a small shoulder at 9 K. The first transition corresponds to an antiferromagnetic

Table 1 Experimental molar heat capacities of ferrosilite, $Fe_2Si_2\ O_6$

T (K)	C_p (J mol^{-1} K^{-1})	T (K)	C_p (J mol^{-1} K^{-1})	T (K)	C_p (J mol^{-1} K^{-1})
PPMS 1st series					
2.028	0.136(2)	10.48	4.58(2)	77.16	48.14(28)
2.029	0.135(2)	10.49	4.58(2)	77.30	48.71(28)
2.032	0.141(2)	10.49	4.58(2)	77.31	48.62(31)
2.206	0.161(2)	11.62	4.98(2)	85.72	55.23(32)
2.208	0.162(2)	11.64	4.98(2)	85.86	55.59(31)
2.209	0.163(2)	11.66	4.98(2)	85.86	55.57(33)
2.400	0.196(3)	12.93	5.44(2)	95.21	62.66(33)
2.402	0.196(3)	12.94	5.44(2)	95.36	62.90(32)
2.404	0.197(3)	12.94	5.44(2)	95.37	62.89(34)
2.613	0.242(4)	14.36	5.94(3)	105.80	71.04(40)
2.617	0.238(4)	14.37	5.95(2)	105.93	71.52(34)
2.619	0.242(4)	14.37	5.95(2)	105.93	71.53(37)
2.843	0.291(5)	15.94	6.54(3)	117.55	80.37(43)
2.847	0.290(5)	15.96	6.56(2)	117.67	80.51(36)
2.85	0.30(1)	15.96	6.56(2)	117.68	80.36(38)
3.10	0.34(1)	17.70	7.34(3)	130.60	89.88(42)
3.10	0.35(1)	17.73	7.37(3)	130.72	89.64(35)
3.10	0.35(1)	17.73	7.37(3)	130.73	90.07(43)
3.37	0.42(1)	19.66	8.31(3)	145.17	99.85(40)
3.38	0.44(1)	19.69	8.35(3)	145.24	99.74(36)
3.38	0.46(1)	19.69	8.35(3)	145.25	99.88(38)
3.67	0.62(1)	21.82	9.66(4)	161.21	109.71(54)
3.68	0.64(1)	21.85	9.72(3)	161.30	109.89(36)
3.68	0.63(1)	21.85	9.71(3)	161.32	110.00(46)
3.99	0.79(2)	24.23	11.45(5)	179.22	120.50(55)
4.00	0.82(1)	24.28	11.70(6)	179.24	120.26(36)
4.01	0.83(1)	24.28	11.54(4)	179.24	120.48(38)
4.35	0.99(2)	26.92	14.15(7)	199.12	130.84(38)
4.36	1.07(2)	26.97	14.28(6)	199.12	131.03(40)
4.36	1.10(2)	26.97	14.27(6)	199.13	131.96(40)
4.74	1.37(2)	29.90	18.01(9)	221.20	142.29(41)
4.75	1.41(2)	29.97	18.22(8)	221.20	142.35(42)
4.76	1.43(2)	29.97	18.20(8)	221.23	143.01(48)
5.01	1.75(2)	33.22	23.79(10)	245.51	154.00(51)
5.03	1.80(2)	33.30	24.14(11)	245.60	153.86(46)
5.04	1.80(1)	33.31	24.15(11)	245.62	154.05(58)
5.16	1.71(3)	37.01	35.01(19)	272.63	168.54(61)
5.17	1.73(3)	37.02	35.01(19)	272.75	168.37(54)
5.18	1.80(2)	37.02	35.03(19)	272.77	168.69(63)
5.59	2.18(2)	41.10	24.90(11)	302.93	177.11(58)
5.59	2.19(2)	41.13	24.95(12)	303.01	177.37(52)
5.59	2.19(2)	41.13	24.94(11)	303.03	177.32(66)
6.20	2.58(2)	45.61	26.48(15)		
6.21	2.59(2)	45.70	26.74(15)		
6.21	2.59(2)	45.70	26.73(16)		
6.88	2.98(2)	50.65	29.35(20)		
6.90	3.01(2)	50.77	29.66(18)		
6.92	3.05(2)	50.77	29.70(19)		
7.65	3.39(2)	56.28	33.19(20)		
7.65	3.39(2)	56.39	33.55(20)		
7.65	3.38(2)	56.39	33.56(21)		
8.49	3.80(2)	62.52	37.45(23)		
8.50	3.80(2)	62.64	37.79(23)		
8.50	3.78(2)	62.65	37.82(24)		
9.43	4.17(2)	69.45	42.68(27)		
9.44	4.17(2)	69.58	43.05(26)		
9.44	4.17(2)	69.59	43.01(27)		
PPMS 2nd series					
30.30	18.92(13)	37.87	40.73(32)	47.32	27.95(21)
30.30	18.90(13)	37.87	40.71(32)	47.92	28.23(18)
30.34	19.11(13)	38.35	41.44(23)	47.94	28.29(21)
30.68	19.57(20)	38.36	41.33(24)	47.94	28.26(20)
30.69	19.44(13)	38.36	41.31(24)	48.55	28.60(19)
30.70	19.44(11)	38.86	31.04(35)	48.58	28.68(21)

Table 1 (Contd.)

T (K)	C_p (J mol^{-1} K^{-1})	*T* (K)	C_p (J mol^{-1} K^{-1})	*T* (K)	C_p (J mol^{-1} K^{-1})
31.06	20.16(23)	38.86	31.01(35)	48.58	28.63(21)
31.11	20.25(14)	38.88	30.78(34)	49.19	28.95(19)
31.11	20.20(13)	39.38	26.46(9)	49.22	29.01(22)
31.52	20.93(14)	39.39	26.50(12)	49.22	29.01(21)
31.53	21.00(14)	39.39	26.49(11)	49.84	29.39(20)
31.53	20.99(14)	39.90	25.64(12)	49.87	29.46(22)
31.93	21.69(14)	39.91	25.67(14)	49.87	29.47(22)
31.94	21.76(15)	39.91	25.69(14)	50.50	29.77(20)
31.94	21.77(15)	40.42	25.30(13)	50.52	29.85(23)
32.35	22.46(15)	40.44	25.35(15)	50.52	29.85(23)
32.36	22.54(15)	40.44	25.34(15)		
32.36	22.54(15)	40.96	25.17(14)		
32.78	23.29(16)	40.97	25.19(16)		
32.79	23.39(16)	40.97	25.23(16)		
32.79	23.38(16)	41.50	25.16(15)		
33.21	24.15(17)	41.51	25.26(16)		
33.22	24.26(16)	41.51	25.21(16)		
33.22	24.26(16)	42.05	25.27(15)		
33.65	25.11(17)	42.06	25.32(17)		
33.66	25.23(17)	42.06	25.34(17)		
33.66	25.24(17)	42.60	25.43(16)		
34.09	26.12(18)	42.62	25.51(17)		
34.10	26.24(18)	42.62	25.50(17)		
34.10	26.25(18)	43.16	25.62(16)		
34.53	27.23(18)	43.18	25.68(18)		
34.55	27.35(19)	43.18	25.71(18)		
34.55	27.37(19)	43.73	25.90(16)		
34.99	28.44(19)	43.75	25.92(18)		
35.01	28.59(20)	43.75	25.94(18)		
35.01	28.59(20)	44.31	26.16(17)		
35.45	29.83(20)	44.33	26.22(19)		
35.47	29.97(21)	44.33	26.24(18)		
35.47	29.96(21)	44.89	26.44(17)		
35.92	31.31(21)	44.91	26.53(19)		
35.94	31.47(22)	44.91	26.53(19)		
35.94	31.46(22)	45.48	26.81(17)		
36.39	32.99(23)	45.50	26.88(19)		
36.41	33.16(23)	45.50	26.89(19)		
36.41	33.17(23)	46.08	27.14(17)		
36.87	34.98(25)	46.10	27.25(20)		
36.89	35.14(26)	46.10	27.25(20)		
36.89	35.14(26)	46.69	27.54(18)		
37.36	37.36(28)	46.71	27.60(20)		
37.38	37.60(29)	46.71	27.59(20)		
37.38	37.61(29)	47.30	27.89(18)		
37.85	40.43(31)	47.32	27.96(21)		
DSC					
343.15	190.79(68)	608.15	237.56(1.44)		
348.15	192.16(59)	613.15	238.10(1.54)		
353.15	193.53(60)	618.15	238.78(1.58)		
358.15	194.84(57)	623.15	239.35(1.71)		
363.15	196.11(52)	643.15	241.10(1.02)		
368.15	197.35(56)	648.15	241.68(94)		
373.15	198.61(63)	653.15	242.13(86)		
378.15	199.82(59)	658.15	242.59(87)		
383.15	200.99(64)	663.15	243.05(91)		
388.15	202.15(65)	668.15	243.52(96)		
393.15	203.32(68)	673.15	243.92(99)		
398.15	204.47(73)	678.15	244.42(93)		
403.15	205.53(75)	683.15	244.79(1.00)		
408.15	206.61(82)	688.15	245.29(1.03)		
413.15	207.70(92)	693.15	245.57(1.13)		
418.15	208.78(91)	698.15	246.09(1.13)		
423.15	209.78(98)	703.15	246.62(1.10)		

Table 1 (Contd.)

T (K)	C_p (J mol^{-1} K^{-1})	T (K)	C_p (J mol^{-1} K^{-1})	T (K)	C_p (J mol^{-1} K^{-1})
443.15	213.56(90)	708.15	247.21(1.11)		
448.15	214.45(83)	713.15	247.77(1.28)		
453.15	215.32(85)	718.15	248.42(1.43)		
458.15	216.23(87)	723.15	249.13(1.55)		
463.15	217.14(82)	743.15	251.66(1.07)		
468.15	217.95(80)	748.15	252.23(1.14)		
473.15	218.82(79)	753.15	252.76(1.06)		
478.15	219.61(82)	758.15	253.38(1.11)		
483.15	220.51(83)	763.15	253.96(1.10)		
488.15	221.33(95)	768.15	254.46(1.05)		
493.15	222.10(91)	773.15	254.96(1.18)		
498.15	222.87(98)	778.15	255.70(1.12)		
503.15	223.69(1.06)	783.15	256.18(1.14)		
508.15	224.50(1.10)	788.15	256.57(1.13)		
513.15	225.26(1.13)	793.15	257.07(1.31)		
518.15	226.04(1.24)	798.15	257.62(1.30)		
523.15	226.84(1.29)	803.15	258.17(1.54)		
543.15	229.57(1.11)	808.15	258.83(1.46)		
548.15	230.05(1.00)	813.15	259.67(1.60)		
553.15	230.74(1.02)	818.15	260.45(1.67)		
558.15	231.34(82)	823.15	261.12(1.98)		
563.15	232.13(91)				
568.15	232.56(83)				
573.15	233.23(91)				
578.15	233.84(1.00)				
583.15	234.43(96)				
588.15	235.05(99)				
593.15	235.72(1.06)				
598.15	236.38(1.20)				
603.15	236.88(1.30)				

ordering of Fe^{2+} spins into a collinear structure. The second transition is due to spin-canting. The two transitions were described using neutron diffraction, magnetisation and magnetic susceptibility measurements (Ghose et al. 1988). Their temperatures of transition are 40 and 8 K, respectively. An alternative possible explanation is that the shoulder around 9 K represents a Schottky anomaly (e.g. Gopal 1966).

The DSC data presented in Table 1 are averages of five scans. In order to derive a C_p polynomial, the data from all scans, along with PPMS data down to 200 K, were used for the fitting procedure. A C_p polynomial as proposed by Berman and Brown (1985) was used, because this polynomial ensures reliable extrapolation to temperatures above the experimental range. The fitting procedure yielded the following expression:

$$C_p\left[\mathrm{J\,mol^{-1}K^{-1}}\right] = 371.75 - 3219.2T^{-1/2} - 15.199 \times 10^5 T^{-2} + 20.704 \times 10^7 T^{-3} \quad (1)$$

with an absolute average deviation of 0.74 J mol^{-1} K^{-1}.

Integrating the C_p versus T and C_p/T versus T curve in the temperature range between 0 and 298.15 K gives the heat content value $[H_{298} - H_0]$ of 28.6 ± 0.1 kJ mol^{-1} and the standard conventional entropy value $[S_{298} - S_0]$ of 186.5 ± 0.5 J mol^{-1} K^{-1}, respectively.

Excess heat capacity and magnetic entropy of ferrosilite

In order to separate the heat capacity contribution of the magnetic transition from the total heat capacity, the procedure described by Robie et al. (1982b) was used. This was done in the following way: using the entropy data for enstatite, $Mg_2Si_2O_6$, (Krupka et al. 1985) in the range from 5 to 380 K, the ratio T/T^* was calculated, where T^* designates the temperature at which the quantity $\left[S^{\mathrm{meas}}_{\mathrm{Fe_2Si_2O_6}} - 2 \times R \ln 5\right]$ is the same as the entropy of enstatite at temperature T, and $S^{\mathrm{meas}}_{\mathrm{Fe_2Si_2O_6}}$ is the entropy obtained from the experimentally determined heat capacities (Fig. 3). The term $2 \times R \ln 5$ in the square brackets gives the limiting value for the magnetic entropy at high temperatures (see Fig. 4). The ratio T/T^* was then plotted against the temperature T. Above ca. 140 K, the ratio T/T^* becomes a linear function of temperature and can be described by the following equation: $T/T^* = 1.2323 - 1.888 \times 10^{-4} \times T$. This equation was then used to extrapolate T/T^* to 0 K and to estimate the lattice entropy of ferrosilite as a function of temperature. In order to obtain the entropy associated with the magnetic transition, the estimated lattice entropies were subtracted from those that were calculated from the experimentally determined heat capacity

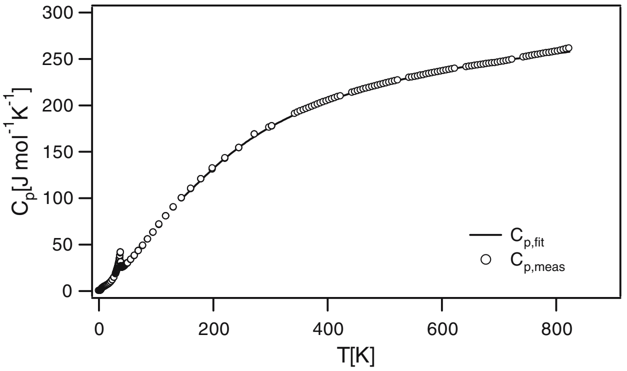

Fig. 1 Experimental molar heat capacity of ferrosilite, $Fe_2Si_2O_6$

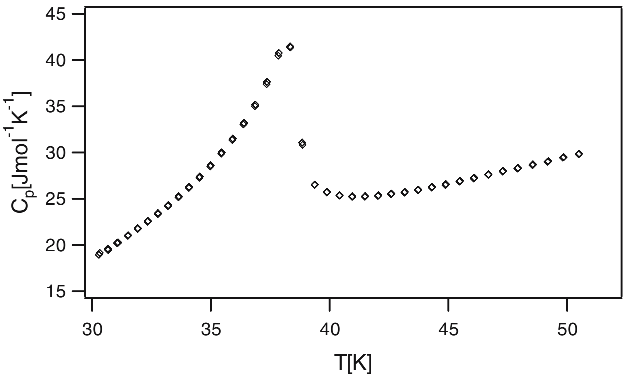

Fig. 2 Experimental molar heat capacity of ferrosilite in the temperature region between 30 and 50 K

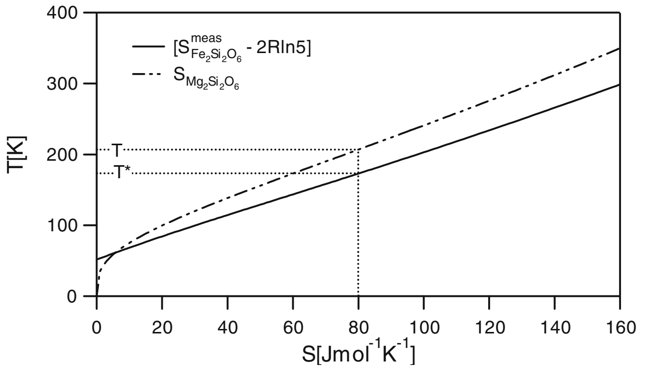

Fig. 3 Entropy of enstatite, $Mg_2Si_2O_6$, and the quantity $[S^{meas}_{Fe_2Si_2O_6} - 2R\ln 5]$ as a function of temperature

values. The results of the calculation, as a function of temperature, are shown in Fig. 4. At the temperature of transition (38.7 K), the value of the magnetic entropy is approximately 17 J mol^{-1} K^{-1} . This is 36 % percent less than the theoretically predicted value of 26.76 J mol^{-1} K^{-1} ($2 \times R \ln 5$). Similar behaviour was observed in the case of fayalite (Robie et al. 1982a), where the magnetic entropy was about 81% of the theoretical value at the Néel temperature. The authors interpreted this as resulting from short-range ordering of the spins above the Néel temperature.

Using the relationship:

$$\left(\frac{\partial S_{\mathrm{mag}}}{\partial T}\right)_P = \frac{C_{p,\mathrm{mag}}}{T} \tag{2}$$

the change in heat capacity due to the magnetic transition, $C_{p,\mathrm{mag}}$, was calculated. The results are shown in Fig. 5 (dotted curve).

Bass and Weidner (1984) determined the average shear and longitudinal sound wave velocities, $\bar{v}_s$ and $\bar{v}_l$, for ferrosilite from experimentally determined elastic moduli measurements. Their values read: $\bar{v}_s = 3.62\,\mathrm{km\,s^{-1}}$ and $\bar{v}_l = 6.54\,\mathrm{km\,s^{1}}$ We use these data and calculate the elastic Debye temperature for ferrosilite from the relationship:

$$\Theta_{\mathrm{el}} = \frac{h}{k}\left[\frac{3qN_{\mathrm{A}}\rho}{4\pi M}\right]^{1/3}\bar{v}_m \tag{3}$$

where h and k are Planck's constant and Boltzmann's constant, respectively, N_{A} is Avogadro's number, ρ is density, M is molecular weight and q gives the number of atoms per formula unit. $\bar{v}_m$ is the average sound velocity that can be calculated from the average shear wave velocity and the average longitudinal wave velocity according to (Anderson 1963):

$$\bar{v}_m = \left[\frac{1}{3}\left(\frac{2}{\bar{v}_s^3} + \frac{1}{\bar{v}_l^3}\right)\right]^{-\frac{1}{3}} \tag{4}$$

With these two sound velocity values, an average sound velocity of $\bar{v}_m = 4.03\,\mathrm{km\,s^{1}}$ is obtained. The density of ferrosilite is 4.002×10^3 kg m^{-3}, its molecular weight is 263.86×10^{-3} kg and the formula unit contains 10 atoms. Inserting these data into Eq. 3, yields a Debye temperature, Θ_{el} of 541 K.

Assuming that the Debye temperature does not change significantly between 0 and 80 K, the lattice heat capacity of ferrosilite was calculated from the relationship:

$$C_v \approx C_p = 9qR\left(\frac{T}{\Theta}\right)^3 \int_0^{\Theta/T} \frac{e^x x^4}{(e^x - 1)^2}\mathrm{d}x \tag{5}$$

where $x = hf/kT$ and $\Theta = hf_D/k$. f designates the vibrational frequency of the oscillators. The results of the calculation are shown in Fig. 6 (circles). Over the temperature range of 0–56 K, these data are in excellent agreement with those that were obtained by the method of Robie et al. (1982b). In order to obtain the heat capacity change associated with the magnetic transition, the resulting C_p data were subtracted from the corresponding experimentally determined heat capacities (Fig. 5, circles).

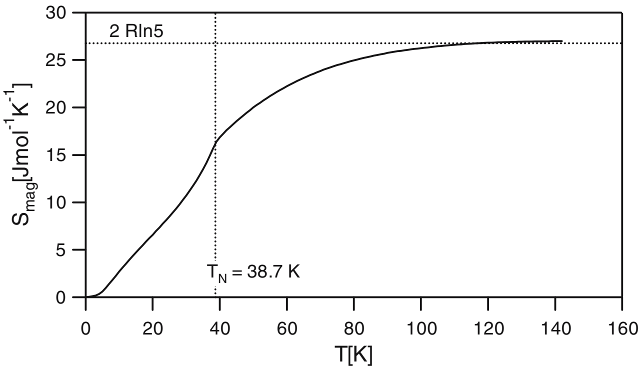

Fig. 4 Magnetic entropy of ferrosilite, $Fe_2Si_2O_6$, as a function of temperature. T_N Néel temperature

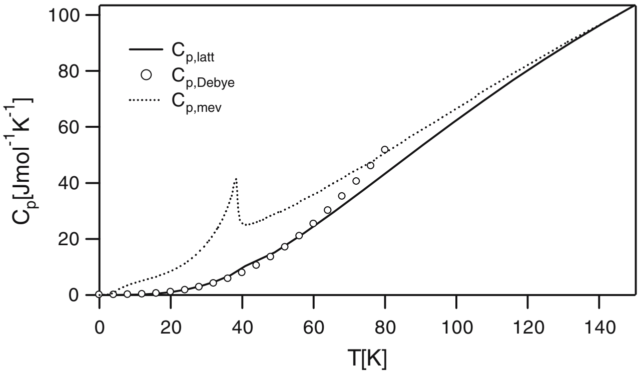

Fig. 5 Molar heat capacity of ferrosilite, $Fe_2Si_2O_6$, in the temperature range between 0 and 200 K. *Solid line* lattice heat capacity calculated using the method of Robie et al. (1982b) and the heat capacity of enstatite. *Dotted line* experimental data, *circles* lattice heat capacity calculated using the elastic Debye temperature

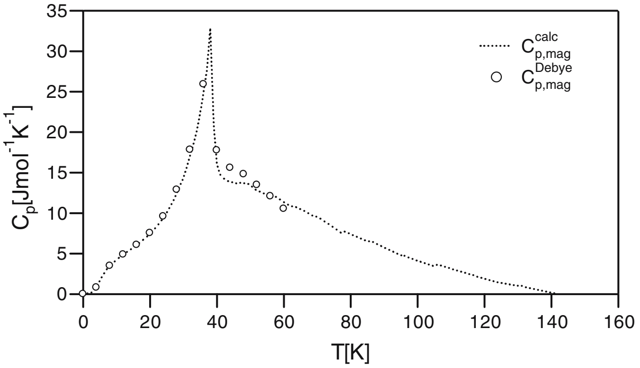

Fig. 6 Heat capacity associated with the magnetic transition. *Dotted curve* calculated using the method of Robie et al. (1982b) and the heat capacity of enstatite to estimate the lattice C_p. *Circles* lattice contribution to C_p estimated using the elastic Debye temperature of ferrosilite

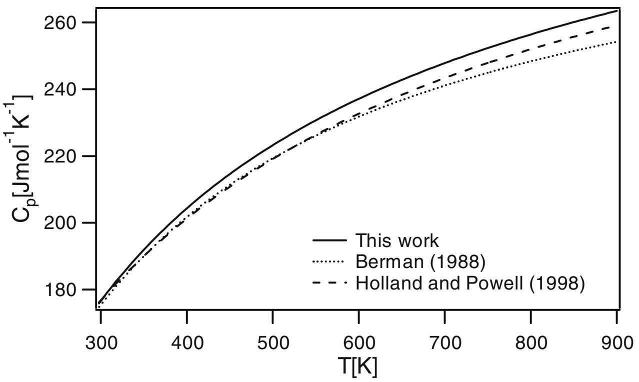

Fig. 7 Molar heat capacity of ferrosilite, $Fe_2Si_2O_6$, above ambient T compared with data in the literature

Discussion

Bohlen et al. (1983) measured the heat capacity of synthetic ferrosilite at temperatures between 8 and 350 K. Only the conventional standard entropy, S_{298} and the temperature of the magnetic transition are given in their publication. Their value for the entropy is 189.12 J mol^{-1} K^{-1} and it is slightly higher than that obtained in this work (186.5 J mol^{-1} K^{-1}).

Polynomials for describing the heat capacity of ferrosilite as a function of temperature above 298 K, as given in the thermodynamic data sets of Berman (1988) and Holland and Powell (1998), are largely based on experimentally determined phase equilibrium data. Berman (1988) uses additionally unpublished C_p measurements of Anovitz.

Figure 7 shows the heat capacity for ferrosilite calculated using the polynomials of these authors and that determined in this study. At room temperature, the three polynomials yield almost identical values. At higher temperatures, however, the C_p versus temperature curves of Berman (1988) and Holland and Powell (1998) deviate from one another and from that of this work. The deviations increase with increasing temperatures. At 600 K, for example, Berman's polynomial yields a C_p value of 231.8 J mol^{-1} K^{-1} . At the same temperature, the polynomial of Holland and Powell (1998) gives 232.7 J mol^{-1} K^{-1} and with the polynomial of this work a value of 237.1 J mol^{-1} K^{-1} is obtained.

Acknowledgments The authors want to thank Mrs. P. Kluge for her technical assistance and C. A. Geiger for reading the manuscript and offering helpful suggestions for improving it. The PPMS measurements were financed by the Austrian Science Fund under project number P15880-N11, which is gratefully acknowledged. Thanks are also due to the reviewers Stephan Klemme and Juraj Majzlan for critical comments that produced a better manuscript.

References

Anderson OL (1963) A simplified method for calculating the Debye temperature from elastic constants. J Phys Chem Solids 24:909–917

Bass JD, Weidner DJ (1984) Elasticity of single-crystal orthoferrosilite. J Geophys Res 89:4359–4371

Berman RG (1988) Internally-consistent thermodynamic data for minerals in the system $Na_2O-K_2O-CaO-MgO-FeO-Fe_2O_3-Al_2O_3-SiO_2-TiO_2-H_2O-CO_2$. J Petrol 29:244–522

Berman RG, Brown TH (1985) Heat capacity of minerals in the system $Na_2O-K_2O-CaO-MgO-FeO-Fe_2O_3-Al_2O_3-SiO_2-TiO_2-H_2O-CO_2$: representation, estimation, and high temperature extrapolation. Contrib Mineral Petrol 89:168–183

Bohlen SR, Metz GW, Essene EJ, Anovitz LM, Westrum EF, Wall VJ (1983) Thermodynamics and phase equilibrium of ferrosilite: potential oxygen barometer in mantle rocks. EOS 64:350

Bosenick A, Geiger CA, Cemič L (1996) Heat capacity measurements of synthetic pyrope-grossular garnet between 320 and 1000 K by differential scanning calorimetry. Geochim Cosmochim Acta 60:3215–3227

Cammenga HK, Eysel W, Gmelin E, Hemminger W, Höhne GWH, Sarge SM (1992) DieTemperaturkalibrierung dynamischer Kalorimeter II. Kalibrierungssubstanzen. PTB Mitteilungen 102:13–18

Dachs E, Bertoldi Ch (2005) Precision and accuracy of the heat-pulse calorimetric technique: low-temperature heat capacities of milligram-sized synthetic mineral samples. Eur J Mineral 17:251–261

Domeneghetti MC, Steffen G (1992) M1, M2 site populations and distortion parameters in synthetic Mg-Fe-orthopyroxenes from Moessbauer spectra and x-ray structure refinements. Phys Chem Miner 19:298–306

Ghose S, Hewat AW, van Dang N, Weidner JR (1988) Magnetic phase transitions in ferrosilite, $Fe_2Si_2O_6$, and hedenbergite, $CaFeSi_2O_6$: Quasi-one dimensional antiferromagnets. EOS Trans Am Geophys Union 69:334

Gopal ESR (1966) Specific heats at low temperatures. Plenum Press, New York

Holland TJB, Powell R (1998) An internally consistent thermodynamic data set for phases of petrological interest. J Metamorph Geol 16:309–343

Hwang JS, Lin KJ, Tien C (1997) Measurement of heat capacity by fitting the whole temperature response of a heat-pulse calorimeter. Rev Sci Instrum 68(1):94–101

Krupka KM, Kerrick DM, Ito J (1985) Low-temperature heat capacities and derived themodynamic properties of anthophyllite, diopside, enstatite, bronzite and wollastonite. Am Mineral 70:249–260

Robie RA, Finch CB, Hemingway BS (1982a) Heat capacity and entropy of fayalite (Fe_2SiO_4) between 5.1 and 383 K: comparison of calorimetric and equilibrium values for the QFM buffer reaction. Am Mineral 67:463–469

Robie RA, Hemingway BS, Takei H (1982b) Heat capacities and entropies of Mg_2SiO_4, Mn_2SiO_4 and Co_2SiO_4 between 5 and 380 K. Am Mineral 67:470–482

Rodriguez-Carvajal J (1990) Fullprof: a program for Rietveld refinement and pattern matching analysis. In: Abstracts of the satelite meeting on powder diffraction of XVth congress of International Union of Crystallography (Toulouse, France) p. 127

Sasaki S, Takeuchi Y, Fujino K, Akimoto S (1982) Electron-density distributions of three orthopyroxenes, $Mg_2Si_2O_6$, $Co_2Si_2O_6$, and $Fe_2Si_2O_6$. Z Kristallogr 158:279–297